Nanotribology and Nanofabrication of MoO$_3$ Structures by Atomic Force Microscopy

Paul E. Sheehan, Charles M. Lieber

Science, New Series, Volume 272, Issue 5265 (May 24, 1996), 1158-1161.

Stable URL:
http://links.jstor.org/sici?sici=0036-8075%2819960524%293%3A272%3C1158%3ANANOMS%3E2.0.CO%3E

of acritarchs, a sign of eutrophic conditions (*26*). Productivity crash followed by productivity boom is a characteristic of oceans in which a rapid decline of circulation rates produces an anoxic lower water column (*27*). Modeling shows that, initially, the productivity declines concomitantly with the decrease of the rate of oceanic overturn and nutrient supply. This effect is counterbalanced by the increased availability of reactive phosphorus (the principal biolimiting nutrient), which is not as efficiently sequestered by iron oxides and organic matter in an anoxic ocean. There is, however, a significant lag time (of the order of tens of thousands of years) between the onset of oceanic anoxia and the build-up of phosphorus (*27*), a delay that is disastrous for the marine biota.

REFERENCES AND NOTES

1. D. H. Erwin, *The Great Paleozoic Crisis* (Columbia Univ. Press, New York, 1993).
2. P. B. Wignall and A. Hallam, *Palaeogeogr. Palaeoclimatol. Palaeoecol.* **93**, 21 (1992).
3. ———, *ibid.* **102**, 215 (1993).
4. Jin Y., Zhu Z., Mei S., *Palaeoworld* **4**, 138 (1994); S. M. Stanley and X. Yang, *Science* **266**, 1340 (1994).
5. P. R. Renne, Zhang Z., M. A. Richards, M. T. Black, A. R. Basu, *Science* **269**, 1413 (1995).
6. A. Hallam, *Hist. Biol.* **5**, 257 (1991); *Can. Soc. Pet. Geol. Mem.* **17**, 797 (1994).
7. M. Gruszczynski, S. Halas, A. Hoffman, K. Malkowski, *Nature* **337**, 64 (1989).
8. K. Nakazawa, K. Nakamura, G. Kimura, *Proc. Jpn. Acad. Sci. B* **63**, 171 (1987); T. Ishibashi and K. Nakazawa, *Mem. Fac. Sci. Kyushu Univ. Ser. D* **26**, 215 (1989).
9. Yin H., Yang F., Zhang K., Yang W., *Mem. Soc. Geol. Ital.* **34**, 329 (1988); H. Kozur, *Zentralbl. Geol. Palaeontol. Teil 1* **11–12**, 1245 (1989); Ding M., in *Permo-Triassic Events in the Eastern Tethys*, W. C Sweet, Z. Yang, J. M. Dickins, H. Yin, Eds. (Cambridge Univ. Press, Cambridge, 1992), pp. 109–119; R. K. Paull and R. A. Paull, *Lethaia* **27**, 271 (1994). An unavoidable consequence of this otherwise commendable choice of P-Tr boundary is that the earliest part of the Griesbachian Stage (defined by the presence of *Otoceras* ammonoids), generally considered to be a basal Triassic age, becomes Permian in age.
10. M. L. Droser and D. J. Bottjer, *J. Sediment. Petrol.* **56**, 558 (1986).
11. P. B. Wignall, H. Kozur, A. Hallam, *Hist. Biol.*, in press.
12. S. U. Noé, *Facies* **16**, 89 (1987); ——— and W. Buggisch, *Jahrb. Geol. Bundesanst. Wien* **137**, 297 (1994).
13. W. T. Holser, H. P. Schönlaub, K. Boeckelmann, M. Magaritz, C. J. Orth, *Abh. Geol. Bundesanst. Wien* **45**, 213 (1991).
14. The evidence includes light pyrite sulfur isotopes diagnostic of syngenetic or early diagenetic formation and trace metal enrichment (V and Ni) typical of black shale environments. One of us (R.J.T.) has examined the core material and found that the Mazzin Member is finely laminated throughout and devoid of the indicators of a supratidal flat (for example, tepees and fenestrae). However, it could be argued that the more distal, basinal setting of the Gartnerkofel site makes it a poor comparison with the generally more proximal localities of the Dolomites, hence the essential need for independent geochemical corroboration from the latter region.
15. J. A. S. Adams and C. E. Weaver, *Am. Assoc. Pet. Geol. Bull.* **42**, 387 (1958); F. B. Zelt, *Soc. Econ. Pal. Min. Field Trip Guidebook* **4**, 49 (1985); K. J. Myers and P. B. Wignall, in *Marine Clastic Environments: New Concepts and Case Studies*, J. K. Legget and G. G. Zuffa, Eds. (Graham and Trotman, London, 1987).
16. C. Broglio Loriga, C. Neri, M. Pasini, R. Posenato, *Mem. Soc. Geol. Ital.* **34**, 5 (1988).
17. R. J. Twitchett and P. B. Wignall, *Palaeogeogr. Palaeoclimatol. Palaeoecol.*, in press.
18. Yang Z. and Li Z., in *Permo-Triassic Events in the Eastern Tethys*, W. C. Sweet, Yang Z., J. M. Dickins, Yin H., Eds. (Cambridge Univ. Press, Cambridge, 1992), pp. 9–20.
19. He J., *Hist. Biol.* **2**, 73 (1989); P. B. Wignall, A. Hallam, Lai X., Yang F., *ibid.* **10**, 175 (1995); P. B. Wignall and A. Hallam, *Palaios*, in press.
20. D. J. Bottjer, M. L. Droser, Wang C., *Geol. Soc. Am. Abstr. Programs* **20**, A106 (1988)
21. R. Brandner, *Ber. Geol. Bund. Wien* **15**, 3 (1988); J. J. Veevers, P. J. Conaghan, S. E. Shaw, *Geol. Soc. Am. Spec. Pap.* **288**, 187 (1994).
22. S. V. Meyen, *Can. Soc. Pet. Geol. Mem.* **2**, 662 (1973); I. A. Dobruskina, *Palaeogeogr. Palaeoclimatol. Palaeoecol.* **58**, 75 (1987); G. Retallack, in *International Geology Congress in Beijing: Abstracts Volume* (in press). The eclectic evidence includes oxygen isotope, fossil plant, and paleosol data.
23. P. W. Hochachka and G. N. Somero, *Biochemical Adaptation* (Princeton Univ. Press, Princeton, NJ, 1984). A 10°C temperature increase doubles the rates of physiological reactions and consequent oxygen requirements.
24. Y. Isozaki, *Can. Soc. Pet. Geol. Mem.* **17**, 805 (1994).
25. M. Magaritz, R. V. Krishnamurthy, W. T. Holser, *Am. J. Sci.* **292**, 727 (1992); K. Wang, H. H. J. Geldsetzer, H. R. Krouse, *Geology* **22**, 580 (1994).
26. B. E. Balme, *Univ. Kansas Spec. Publ.* **4**, 305 (1970); G. J. Retallack, *Science* **267**, 77 (1995).
27. E. D. Ingall, R. M. Bustin, P. van Cappellen, *Geochim. Cosmochim. Acta* **56**, 3323 (1993); P. van Cappellen and E. D. Ingall, *Paleoceanography* **9**, 677 (1994).

28. The Spitsbergen fieldwork was supported by a grant from the Royal Society and the Cambridge Arctic Shelf Programme. The Dolomites fieldwork was supported by a Natural Environment Research Council postgraduate studentship.

16 January 1996; accepted 21 March 1996

Nanotribology and Nanofabrication of MoO_3 Structures by Atomic Force Microscopy

Paul E. Sheehan and Charles M. Lieber*

Atomic force microscopy was used to characterize the sliding of molybdenum oxide (MoO_3) nanocrystals on single-crystal molybdenum disulfide (MoS_2) surfaces. Highly anisotropic friction was observed whereby MoO_3 nanocrystals moved only along specific directions of the MoS_2 surface lattice. The energy per unit area to move the MoO_3 nanocrystals along their preferred sliding direction was an order of magnitude less than required to slide macroscopic MoS_2-bearing contacts. This extreme friction anisotropy was exploited to fabricate multicomponent MoO_3 nanostructures. These reversibly interlocking structures could serve as the basis for devices such as mechanical logic gates.

Three centuries of macroscopic studies of friction, adhesion, and wear have contributed much to the phenomenological understanding of tribology (*1*, *2*). However, studies of interactions between macroscopic bodies are influenced by complex factors, including surface roughness and adsorbates, that have precluded the development of a first-principles understanding of friction and adhesion (*2*, *3*). In principle, nanometer-scale measurements of friction and adhesion forces should be interpretable in terms of fundamental intermolecular forces, and such measurements could thus play a central role in the development of microscopic models of friction and the rational design of improved lubricants. Moreover, such microscopic information is highly relevant to the emerging field of nanotechnology, where noncovalent interactions are important in the manipulation, assembly, and stability of new structures.

Atomic force microscopy (AFM) can be used to measure normal (adhesive) and lateral (friction) forces on the nanometer scale, and thus it is a powerful technique for probing the microscopic mechanism of friction (*3*–*8*). Studies of friction between probe tips and different surfaces have yielded a number of interesting observations, including atomic scale stick-slip motion (*4*, *6*) and functional-group dependence of friction (*7*, *8*). These studies have also raised the issues of whether friction depends on the crystallographic direction of sliding and whether the contact between an AFM microscope probe tip and a surface is a single- or multiple-asperity contact (*9*, *10*).

These issues highlight a principal weakness of AFM for tribology: The structure of the probe tip–sample sliding interface may not be well defined, even though the probe tip can provide nanometer-scale resolution. Here, we eliminated this essential uncertainty by probing the friction of MoO_3 nanocrystals sliding on single-crystal MoS_2. This system is well suited for nanotribology studies because the interface structure and contact area are atomically defined and because the MoO_3

Department of Chemistry and Division of Applied Sciences, Harvard University, Cambridge, MA 02138, USA.

*To whom correspondence should be addressed.

nanocrystals can be moved controllably with the AFM microscope tip. We found that the measured friction is extremely anisotropic, with MoO_3 crystals sliding along only one of the three equivalent MoS_2 surface directions. We then developed an atomic model of the interface to explain these observations. We compared the energetics of the sliding process, as determined from measurements of the friction as a function of nanocrystal contact area, with macroscopic data reported for this widely used lubricant system. Finally, we assembled interlocking nanostructures by exploiting the extreme anisotropy in the sliding of the crystals.

The growth and characterization of MoO_3 nanocrystals on single-crystal MoS_2 surfaces has been described (*11*). Briefly, oxidation of single-crystal 2*H*-MoS_2 surfaces produces nanocrystals of α-MoO_3, one to five unit cells thick, oriented with the *a* and *c* axes parallel to the (0001) MoS_2 surface. An AFM microscope (Nanoscope III, Digital Instruments) image of three MoO_3 nanocrystals, obtained with a Si_3N_4 tip in a nitrogen-filled Chamber equipped with a system for H_2O and O_2 removal (*11*), is shown in Fig. 1A. The MoO_3 nanocrystals are immobile when they are imaged with small loads. However, when the applied load exceeds a size-dependent critical value (see below), the scanning-imaging process moves the two smaller nanocrystals along the MoS_2 surface. Images of the static positions of these nanocrystals were recorded after they were moved by 92 sequential high-load (47 nN) horizontal scans (Fig. 1B) and then moved a second time by 66 sequential high-load horizontal scans (Fig. 1C); these images show that the two nanocrystals move downward along distinct paths. A composite of the three images (Fig. 1D) highlights these features and provides further insight into the nature of sliding in this system. First, analysis of the relative sliding directions of the two nanocrystals shows that they moved at a 60° angle with respect to each other. Second, atomic periodicity images of the hexagonal MoS_2 substrate lattice recorded during these experiments show that the observed sliding directions coincided with crystal lattice directions. In all cases examined to date, we have found that the MoO_3 nanocrystals only move along a single preferred direction, and that this direction always coincides with one of the equivalent lattice directions of the MoS_2 substrate; hence, we term this motion lattice-directed sliding.

The friction anisotropy in the MoO_3-MoS_2 system is extreme relative to the results of previous studies (*6*, *9*, *12*–*14*): In-plane forces applied perpendicular to and

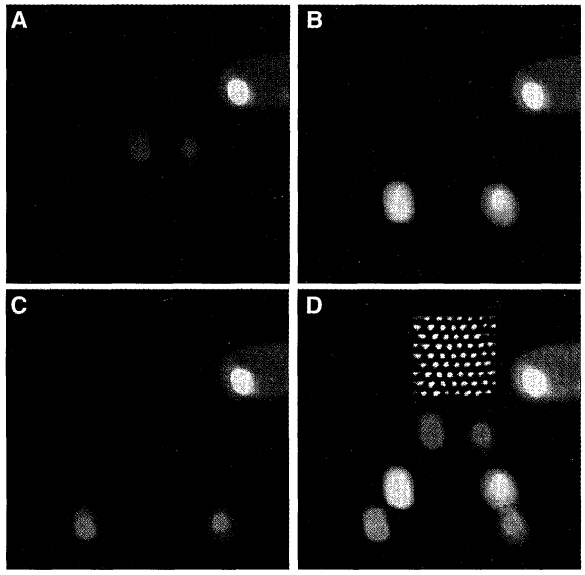

Fig. 1. Images of MoO_3 nanocrystals on a MoS_2 substrate. (**A**) Initial positions of two small MoO_3 nanocrystals (pink) and one larger nanocrystal (gray). (**B**) Positions of the two small nanocrystals (yellow) after they were moved by 92 sequential high-load horizontal scans. (**C**) Final positions of the two small nanocrystals (blue) after they were moved a second time by 66 additional high-load scans. (**D**) Composite image illustrating the relative positions of the nanocrystals in (A), (B), and (C). The inset shows the atomic lattice of the MoS_2 substrate; its orientation reflects that of the substrate in all four images. Translation of the nanocrystals was initiated by increasing the applied load to 47 nN at the beginning (top) of the scan area (512 by 512 pixels) and was terminated by decreasing the load to ~0 nN. The displayed images were acquired after the translation step with an applied load of ~0 nN. The image sizes are 420 nm by 420 nm; the inset in (D) is 2 nm by 2 nm.

an order of magnitude greater than those required for sliding along the preferred lattice direction failed to move MoO_3 nanocrystals. Large perpendicular forces can, however, lead to wear and nanomachining of the MoO_3 (*11*). Studies of sliding between macroscopic diamond crystal surfaces showed a maximum anisotropy between different crystallographic directions of ~2 at large loads, although at smaller applied loads there was no friction anisotropy (*12*). Examination of the worn diamond surfaces after these measurements suggested that the observed friction anisotropy was a result of the varying energetics of crack formation and plastic deformation of the surface (along different crystal directions). This mechanism of friction anisotropy cannot explain our results, because there is no wear of the MoO_3-MoS_2 interface. Studies of friction between macroscopic mica contacts have also exhibited friction anisotropy of up to a factor of four between different crystal directions (*13*). This friction anisotropy was attributed to the degree of commensurability between the contacting mica lattices (because no surface wear was detected) and thus may be similar to our results.

To probe the possibility that lattice commensurability may cause the extreme friction anisotropy observed here, we examined models of the MoO_3-MoS_2 interface that incorporate (i) the known structures of the MoS_2 and MoO_3 lattices, (ii) the observation from atomic periodicity images that the MoO_3 *a* axis is rotated ~14° with respect to the MoS_2 *a* axis, and (iii) the lattice-directed sliding effect (*15*). The model shown in Fig. 2 qualitatively explains the friction anisotropy for sliding MoO_3 nanocrystals on MoS_2. In this model, the MoO_3 surface atoms can slide in one direction, in channels defined by the sulfur atom rows of the MoS_2 surface. In contrast, motion along the other two equivalent MoS_2 lattice directions requires interfacial atoms to pass directly over each other. This crossing should lead to a more corrugated potential along these directions (*14*, *16*), and thus to a larger friction. Although quantitative calculations have not been reported for the MoO_3-MoS_2 system, molecular dynamics simulations of friction between two diamond surfaces have produced a similar effect (*14*).

The lattice-directed sliding of MoO_3

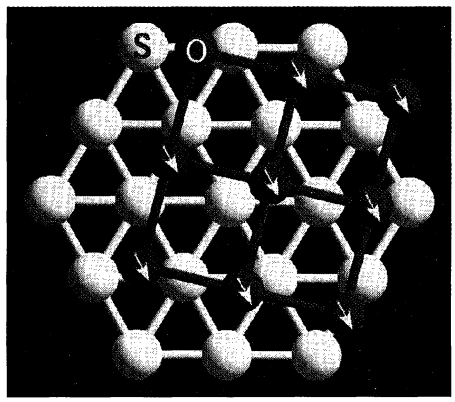

Fig. 2. Computer model of the atomic structure of the MoO_3-MoS_2 interface. The preferred sliding direction, which enables the MoO_3 surface atoms to slide between rows of sulfur atoms, is indicated by arrows on atoms of the MoO_3 lattice. The lattices shown correspond to those of bulk crystals. Because our imaging studies show that the atomic periodicities of these surfaces are the same as the bulk periodicity (as expected for layered solids), we believe that these structures are a good approximation of the contacting surfaces.

nanocrystals over single-crystal MoS_2 provides a unique opportunity to study friction under highly controlled conditions because the interface between the two surfaces is atomically defined and maintains its orientation while moving (*17*). To study the friction in our system, we measured the minimum lateral force needed to move the MoO_3 nanocrystals along their preferred sliding axis as a function of nanocrystal area (Fig. 3). In these experiments, we scanned the tip on the MoS_2 surface at the preferred sliding direction of a particular MoO_3 nanocrystal (sample frame of reference), contacted the edge, and then moved the nanocrystal. The measured lateral force is equal to the sum of the friction between the tip-MoS_2 and MoO_3-MoS_2 interfaces; the tip-MoS_2 contribution, which is measured before contact, is typically an order of magnitude smaller than the MoO_3-MoS_2 value and is thus readily subtracted from the measured sum. We found a good linear correlation between the static friction force and the nanocrystal area. This correlation is strong evidence that the friction force is directly proportional to the number of atomic interactions at the MoO_3-MoS_2 interface. From the slope of these data, we calculated the shear stress s (friction force divided by area) for sliding MoO_3 on MoS_2 and obtained a value of 1.1 MPa. Although s is expressed in macroscopic units, in our system it can be considered a microscopic variable because the sliding interface structure and area are well defined (*18*). Indeed, we believe that this system is an ideal one to compare with theory, where it should be possible to calculate s in the limit of a single unit cell contact.

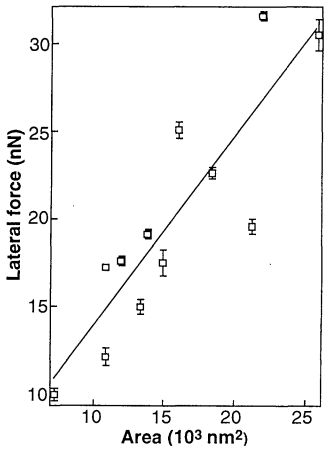

Fig. 3. Plot of the lateral friction force needed to move the MoO_3 nanocrystals along the preferred sliding direction as a function of nanocrystal area. The minimum lateral force for sliding was determined by increasing the load until the tip pushed (rather than imaged) the MoO_3 nanocrystal. The lateral force contribution from friction of the tip on the MoS_2 surface was a small contribution to the overall measured force and was subtracted from the total in these measurements. The procedures used to measure quantitatively lateral forces have been described (*7*).

Because MoS_2 is a widely used solid lubricant, we compared our well-defined value of s for the MoO_3-MoS_2 system with values of s determined from macroscopic friction measurements of MoS_2. Comprehensive friction studies of MoS_2 thin films in dry air have yielded $s = 24.8 \pm 0.5$ MPa (*19*). This macroscopic value of s is 20 times our value for the preferred sliding direction of the MoO_3-MoS_2 system. Consideration of the friction (and hence s) anisotropy observed in our microscopic studies suggests that the much larger average value of s found in macroscopic measurements arises in part from motion along high-energy pathways. Indeed, if it were possible to align atomically the sliding interface between macroscopic objects such as bearings, friction would be markedly reduced. Alternatively, it might be possible to exploit this reduced friction in producing micro- or nanomachines that are much more efficient than can be predicted from macroscopic considerations. The value of s determined for MoO_3-MoS_2 can also be compared with recent studies of C_{60} islands sliding on NaCl crystal surfaces (*20*). The shear stress determined from sliding a C_{60} island on NaCl, $s = 0.1$ MPa, is one-tenth of our value for MoO_3-MoS_2. Part of this difference may reflect differences in lattice commensurability and the molecular nature of the C_{60} solid, although further experimental and theoretical studies are needed to provide a quantitative explanation of the large difference in s.

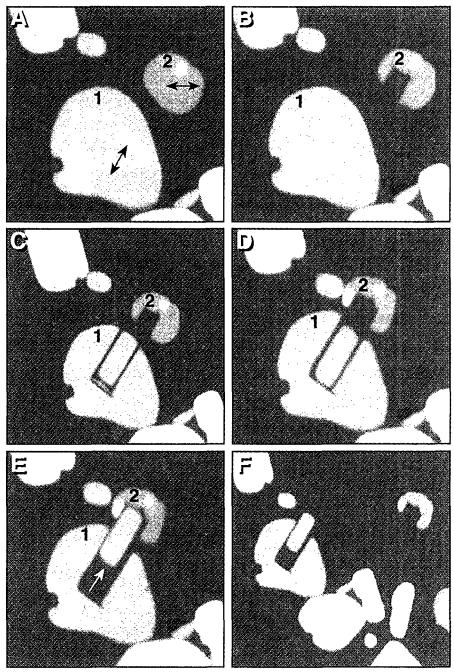

Fig. 4. Images of selected steps in the fabrication of a nanostructure containing three interlocking pieces. (**A**) Initial positions of two MoO_3 nanocrystals, crystal 1 and crystal 2 (the preferred sliding directions are indicated by two-headed arrows). (**B**) A 52-nm notch was defined in crystal 2 by nanomachining (*11*). (**C**) A 58-nm free rectangle (latch) was machined in crystal 1, and crystal 2 was translated toward crystal 1. (**D**) Crystal 2 was translated to align the notch with the latch. (**E**) The latch was moved into the notch of crystal 2. (**F**) The latch was broken after a force of 41 nN was applied to the latch axis. The nanomachining steps used to define the notch and latch were carried out with an applied load of 95 nN, and all images were recorded with an applied load of ~0 nN. Image sizes are 600 nm by 600 nm, except for (F), which is 900 nm by 900 nm.

The large friction anisotropy in the MoO_3-MoS_2 system also has important implications for nanofabrication. By combining lattice-directed sliding with nanomachining (*11*), it is possible to define, interconnect, and lock nanocrystals together (Fig. 4). To illustrate this point, we used two MoO_3 nanocrystals that have different preferred sliding directions on the MoS_2 substrate (Fig. 4A). First, we opened a 52-nm notch in the smaller nanocrystal (crystal 2) by nanomachining (Fig. 4B). Second, we defined a rectangular latch in the larger nanocrystal (crystal 1) and translated crystal 2 so that its notch was almost aligned with this latch (Fig. 4C). At this stage of fabrication, we enlarged the notch by 11 nm so that it was wider than the 58-nm latch, and we adjusted the position of crystal 2 to be diametrically opposed to the latch (Fig. 4D). By sliding the latch into the notch of crystal 2 (Fig. 4E), we effectively locked the two nanocrystals, because crystal 2 could no longer move along its preferred sliding direction of the MoS_2 substrate. Hence, we created a nanometer-scale mechanical lock. Such locking is reversible; after recording the image in Fig. 4D, we locked and unlocked crystals 1 and 2 several times before recording the image in Fig. 4E. We also tested the strength of the latch by determining the force required to slide crystal 2 perpendicular to the latch axis (Fig. 4F). The lateral force needed to break the latch, 41 nN, was large considering the small latch contact area, which suggests that relatively robust assemblies can be created with such devices. Such a reversible latch could serve as the basis for mechanical logic gates (*21*). More generally, we believe that our results represent an important step toward the creation of nanometer-scale devices, because they demonstrate the ability to machine complex shapes and to reversibly assemble these pieces into interlocking structures.

REFERENCES AND NOTES

1. G. Amontons, *Mem. Acad. R. Sci.* 206 (1699); F. P. Bowden and D. Tabor, *The Friction and Lubrication of Solids* (Clarendon, Oxford, 1964), part II.
2. *Fundamentals of Friction: Macroscopic and Micro-*

scopic Processes, I. L. Singer and H. M. Pollock, Eds. (Kluwer, Dordrecht, Netherlands, 1992).
3. I. L. Singer, *J. Vac. Sci. Technol.* **A12**, 2605 (1994); B. Bhushan, J. N. Israelachvili, U. Landman, *Nature* **374**, 607 (1995).
4. C. M. Mate, G. M. McClelland, R. Erlandsson, S. Chiang, *Phys. Rev. Lett.* **59**, 1942 (1987).
5. N. A. Burnham, D. D. Dominguez, R. L. Mowery, R. J. Colton, *ibid.* **64**, 1931 (1990); G. S. Blackman, C. M. Mate, M. R. Philpott, *ibid.* **65**, 2270 (1990); G. J. German *et al.*, *J. Appl. Phys.* **73**, 163 (1993).
6. R. M. Overney, H. Takano, M. Fujihara, W. Paulus, H. Ringsdorf, *Phys. Rev. Lett.* **72**, 3546 (1994).
7. C. D. Frisbie, L. F. Rozsnyai, A. Noy, M. S. Wrighton, C. M. Lieber, *Science* **265**, 2071 (1994); A. Noy, C. D. Frisbie, L. F. Rozsnyai, M. S. Wrighton, C. M. Lieber, *J. Am. Chem. Soc.* **117**, 7943 (1995).
8. R. M. Overney *et al.*, *Langmuir* **10**, 1281 (1994).
9. J. Hu, X.-D. Xiao, D. F. Ogletree, M. Salmeron, *Surf. Sci.* **327**, 358 (1995).
10. M. Binggeli and C. M. Mate, *Appl. Phys. Lett.* **65**, 415 (1994).
11. Y. Kim and C. M. Lieber, *Science* **257**, 375 (1992); Y. Kim, thesis, Harvard University (1993).
12. Y. Enomoto and D. Tabor, *Proc. R. Soc. London Ser. A* **373**, 405 (1981).
13. M. Hirano, K. Shinjo, R. Kaneko, Y. Murata, *Phys. Rev. Lett.* **67**, 2642 (1991).
14. J. A. Harrison, C. T. White, R. J. Colton, D. W. Brenner, *Phys. Rev. B* **46**, 9700 (1992).
15. We assume that the surface of the MoO_3 nanocrystal sliding on MoS_2 has the same rectangular lattice as was observed experimentally at the exposed nanocrystal surface, because only integral multiples of the unit cell (along the *b* axis) were observed in thickness measurements of the MoO_3 nanocrystals. We cannot rule out the substitution of some sulfur into the surface oxygen anion layer, although we believe this is unlikely because the magnitude of the observed friction is much larger than was observed for sliding MoS_2 on a MoS_2 substrate (P. E. Sheehan and C. M. Lieber, unpublished results).
16. L. J. Whitman, J. A. Stroscio, R. A. Dragoset, R. J. Celotta, *Science* **251**, 1206 (1991).
17. The experimental results are only consistent with the atomic interface shown in Fig. 2. No direct method exists to assess the atomic structure of the sliding surface of the MoO_3 nanocrystals.
18. Friction for macroscopic systems is commonly expressed in a load-dependent form, $F = \mu L$, where L is the load and μ is the phenomenological coefficient of friction. In this expression, the friction is apparently independent of the contact area A; in reality, as L is increased between two rough surfaces, the contact area increases. Hence, $F = sA$ represents a more microscopic representation of friction if the contact area is known at the atomic level.
19. I. L. Singer, R. N. Bolster, J. Wegand, S. Fayeulle, B. C. Stupp, *Appl. Phys. Lett.* **57**, 995 (1990).
20. R. Lüthi *et al.*, *Science* **266**, 1979 (1994).
21. K. E. Drexler, *Nanosystems* (Wiley, New York, 1992), p. 364.
22. Supported by the Air Force Office of Scientific Research (F49620-94-1-0010).

16 January 1996; accepted 1 April 1996

GS28, a 28-Kilodalton Golgi SNARE That Participates in ER-Golgi Transport

V. Nathan Subramaniam, Frank Peter, Robin Philp, Siew Heng Wong, Wanjin Hong*

Little is known about the integral membrane proteins that participate in the early secretory pathway of mammalian cells. The complementary DNA encoding a 28-kilodalton protein (p28) of the cis-Golgi was cloned and sequenced. The protein was predicted to contain a central coiled-coil domain with a carboxyl-terminal membrane anchor. An in vitro assay for endoplasmic reticulum–Golgi transport was used to show that p28 participates in the docking and fusion stage of this transport event. Biochemical studies established that p28 is a core component of the Golgi SNAP receptor (SNARE) complex.

The *N*-ethylmaleimide–sensitive factor (NSF) and the soluble NSF attachment proteins (SNAPs) are required for most vesicle fusion events along the exocytotic and endocytotic pathway (*1*). The cytosolic NSF and SNAPs are recruited to the fusion sites through binding to membrane SNAREs. The specificity of vesicular transport is thought to be determined by correct pairing of vesicle-associated SNAREs (v-SNAREs) with those on the target membrane (t-SNAREs) (*1*). Synaptic vesicle–associated synaptobrevins (v-SNAREs) and presynaptic membrane–associated syntaxin 1A and 1B (complexed with SNAP-25) (t-SNAREs) have been shown to interact with each other to determine the specific docking of synaptic vesicles on the presynaptic membrane as well as to recruit SNAPs and subsequently NSF, resulting in the formation of a 20S fusion (or SNARE) complex (*1*, *2*). Although the 20S SNARE complex was originally formed with Golgi membrane extracts in the presence of NSF and α-SNAP (*3*), the Golgi proteins of this SNARE complex have not been identified.

Syntaxin 2, 3, 4, and 5, Sed5p, Sso1p, Sso2p, Pep12p, cellubrevin, Sec22p (Sly2p), Bet1p (Sly12p), Bos1p, Snc1p, Snc2p, and Sft1p are other possible SNAREs that function in different vesicular transport steps (*1*, *4*). Among these, only syntaxin 5 is implicated in endoplasmic reticulum (ER)–Golgi transport in mammalian cells (*5*).

A cis-Golgi integral membrane protein, p28, has recently been identified by a monoclonal antibody (mAb), HFD9 (*6*). The protein was immunoaffinity-purified from a detergent extract of rat liver Golgi-enriched membranes, and the amino acid sequences of its proteolytic peptides were used to isolate the full-length complementary DNA (cDNA) (*7*) (Fig. 1). The deduced amino acid sequence shows that p28 is a 250–amino acid protein. The major portion of the polypeptide (residues 1 to 230) is predicted to be anchored to the membrane by its 20-residue COOH-terminal hydrophobic tail (residues 231 to 250). Preceding the hydrophobic tail are several regions (residues 67 to 94, 101 to 128, 129 to 152, and 163 to 226) that could potentially form coiled-coil domains. The structure of p28 is similar to that of known SNAREs, although the primary sequence of p28 does not show significant similarity to any of them (*1*, *4*).

The structure of p28 and its cis-Golgi localization (*6*) prompted us to examine whether p28 functions in ER to cis-Golgi

Fig. 1. The cDNA and deduced amino acid sequence of p28. Peptide sequences obtained by microsequencing of proteolytic fragments of purified p28 are underlined. The COOH-terminal membrane anchor is boxed. This sequence has been deposited with GenBank (accession no. U49099). Abbreviations for the amino acid residues are as follows: A, Ala; C, Cys; D, Asp; E, Glu; F, Phe; G, Gly; H, His; I, Ile; K, Lys; L, Leu; M, Met; N, Asn; P, Pro; Q, Gln; R, Arg; S, Ser; T, Thr; V, Val; W, Trp; and Y, Tyr.

Membrane Biology Laboratory, Institute of Molecular and Cell Biology, National University of Singapore, 10 Kent Ridge Crescent, Singapore 119260, Singapore.

*To whom correspondence should be addressed.